

SCATTERING FROM MULTIPLE BIANISOTROPIC CYLINDERS AND THEIR MODELING OF CYLINDRICAL OBJECTS OF ARBITRARY CROSS-SECTION

W. Y. Yin, L. W. Li, and M. S. Leong

Department of Electrical Engineering
National University of Singapore
Singapore, 119260

- 1. Introduction**
 - 2. Geometry of the Problem**
 - 3. Field Distribution**
 - 4. Numerical Results and Discussions**
 - 5. Conclusion**
- Appendices**
References

1. INTRODUCTION

It is well known that the electromagnetic scattering of plane and beam waves by various composite cylindrical objects has long been studied by many authors [1–8], and these studies have been motivated both by interest in developing new techniques for solving scattering problems and by numerous engineering applications. For instance, many complex practical problems require a number of composite cylinders to model the scatter environment, improve and control the scattering properties in diverse areas like bioelectromagnetics, microwave remote sensing and imaging, and optical communication, et al. The geometries of cylindrical objects treated before include dielectric or impedance cylinders embedded into another dielectric cylinder as well as two or N parallel conducting and dielectric cylinders. The corresponding approaches used for dealing with these models can be the analytical separation variables technique for circular cross-section, while for

non-separable cylinder cross-section, the numerical techniques, such as extended boundary condition method, moment method as well as finite element method must be adopted.

Furthermore, in the past few years some significant theoretical research progresses have been achieved concerning with the electromagnetic characteristics and potential applications of bianisotropic materials. For instance, (1) the dyadic Green's function for source radiation and wave propagation in bianisotropic media [9–13]; (2) the guided wave features of hybrid modes in some bianisotropic waveguides [14–20]; (3) the dispersion characteristics of multiconductor transmission lines in one- and two-layer grounded bianisotropic superstrate-substrate [21–23], and (4) experimental investigation on the effective constitutive parameters of uniaxial bianisotropic composites [24]. On the other hand, the scattering characteristics of various cylindrical bi(an)isotropic objects has also been examined by some authors, such as the scattering of normally and obliquely incident waves by one or multilayered bi(an)isotropic cylinders of circular or arbitrary cross section using the separation variables technique, moment-method and propagator matrix approach, et al., [25–32]. Also, the multiple scattering from parallel bianisotropic cylinders has been treated recently [33–35].

In this contribution, the generalized model of electromagnetic scattering from a planar array of multiple eccentric bianisotropic cylinders is established and formulated using some hybrid but analytic techniques. Furthermore, numerical calculation is carried out to investigate the multiple scattering features of two-dimensional bianisotropic objects of arbitrary cross section and various effects of constitutive parameters are examined. The motivation for this study is not only for the consideration of academic importance in complex media, but also essential for the potential engineering applications.

2. GEOMETRY OF THE PROBLEM

Fig. 1 shows the cross section of a planar array made of N parallel, infinitely long, multilayered, and internal eccentrically overlapping bianisotropic circular cylinders embedded in an unbounded isotropic medium with permittivity ε_b and permeability μ_b .

The bianisotropic media are usually dissipative and their constitutive characteristics here are assumed to be described by the following relations in an appropriate frequency range ($e^{i\omega t}$):

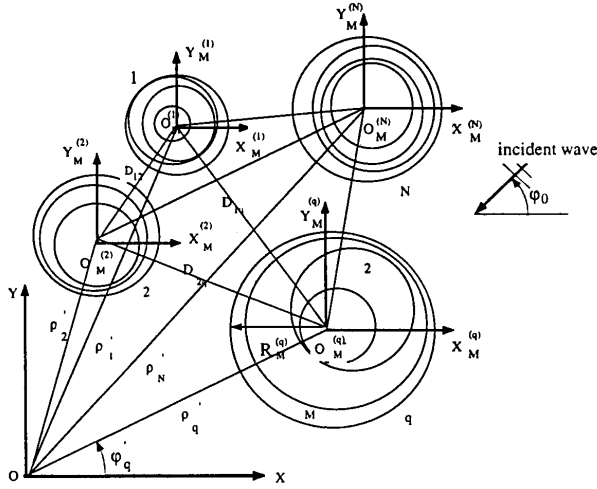


Figure 1. Geometry and coordinates of N ($q = 1, 2, \dots, N$) parallel, M -layer composite eccentric bianisotropic circular cylinders. The separation between cylinders between q and g ($g \neq q, g = 1, 2, \dots, q - 1, q + 1, \dots, N$) is determined by $D_{qg} \geq (R_M^{(q)} + R_M^{(g)})$.

$$\begin{bmatrix} \vec{D}^{(q,p)}(\omega) \\ \vec{B}^{(q,p)}(\omega) \end{bmatrix} = \begin{bmatrix} \begin{bmatrix} \varepsilon_p^{(q)}(\omega) \\ \xi_{ep}^{(q)}(\omega) \end{bmatrix} \\ \begin{bmatrix} \xi_{mp}^{(q)}(\omega) \\ \mu_p^{(q)}(\omega) \end{bmatrix} \end{bmatrix} \begin{bmatrix} \vec{E}^{(q,p)}(\omega) \\ \vec{H}^{(q,p)}(\omega) \end{bmatrix}. \quad (1a, b)$$

where $[\varepsilon_p^{(q)}(\omega)]$, $[\mu_p^{(q)}(\omega)]$, $[\xi_{ep}^{(q)}(\omega)]$, and $[\xi_{mp}^{(q)}(\omega)]$ are the permittivity tensor, permeability tensor, and magnetoelectric cross-coupling tensors, respectively, $p = 1, 2, \dots, M$ (layer number), $q = 1, 2, \dots, N$ (outermost cylinder number). Here, it should be emphasized that the case of electrically large cylinders $\{k R_M^{(q)} \gg 1, k = \omega \sqrt{\mu_b \varepsilon_b}\}$ will not be taken into consideration. The radii of the q th composite cylinder are denoted by $R_1^{(q)}, \dots, R_M^{(q)}$, and their respective axes are fixed at the origins $O_1^{(q)}, \dots, O_M^{(q)}$, respectively. The eccentric distances from $O_2^{(q)}, \dots, O_M^{(q)}$ to $O_1^{(q)}$ are denoted by $d_{p1}^{(q)}$ ($p = 2, \dots, M$), and the four constitutive tensors of the q th bianisotropic cylinder in the p th layer are supposed to be described by the following gyrotropic form in the cylindrical coordinate system $O_p^{(q)}(\rho_p^{(q)}, \varphi_p^{(q)}, z_p^{(q)})(\rho_p^{(q)} \leq R_p^{(q)})$,

$$\left[C_p^{(q)}(\omega) \right] = \begin{bmatrix} C_1^{(q,p)}(\omega) & iC_{12}^{(q,p)}(\omega) & 0 \\ -iC_{12}^{(q,p)}(\omega) & C_1^{(q,p)}(\omega) & 0 \\ 0 & 0 & C_2^{(q,p)}(\omega) \end{bmatrix}, \quad C = \varepsilon, \mu, \xi_e, \xi_m. \quad (2)$$

where $\left[C_p^{(q)}(\omega) \right]$ is of sufficient generality and can incorporate most practical applications. For instance, when $C_{12}^{(q,p)}(\omega) = 0$, (2) just stands for the uniaxial bianisotropic media (UBM), and when $\left[\xi_{ep,mp}^{(q)}(\omega) \right] = 0\bar{I}$, it become the ordinary gyroelectromagnetic media, here \bar{I} is the unit dyad. Especially, according to the symmetry theory of the continuous group [36–38], (2) is also reasonable for describing the constitutive features of Faraday chiral media (FCM), i.e., chiroplasmas and chiroferrites [39, 40]. Corresponding to the different magnetic groups, the magnetoelectric cross-coupling tensors $\left[\xi_{ep,mp}^{(q)}(\omega) \right]$ may be chosen to be of the following forms [36]:

$$1^\circ(C_\infty) : \begin{bmatrix} \xi_{ep}^{(q)} \\ \xi_{mp}^{(q)} \end{bmatrix} = \begin{bmatrix} \xi_{e1}^{(q,p)} & \xi_{e12}^{(q,p)} & 0 \\ -\xi_{e12}^{(q,p)} & \xi_{e1}^{(q,p)} & 0 \\ 0 & 0 & \xi_{e2}^{(q,p)} \end{bmatrix}, \quad \begin{bmatrix} \xi_{m1}^{(q,p)} & \xi_{m12}^{(q,p)} & 0 \\ -\xi_{m12}^{(q,p)} & \xi_{m1}^{(q,p)} & 0 \\ 0 & 0 & \xi_{m2}^{(q,p)} \end{bmatrix}, \quad (3a)$$

$$2^\circ(D_\infty) : \begin{bmatrix} \xi_{ep}^{(q)} \\ \xi_{mp}^{(q)} \end{bmatrix} = \begin{bmatrix} \xi_{e1}^{(q,p)} & \xi_{e12}^{(q,p)} & 0 \\ -\xi_{e12}^{(q,p)} & \xi_{e1}^{(q,p)} & 0 \\ 0 & 0 & \xi_{e2}^{(q,p)} \end{bmatrix}, \quad \begin{bmatrix} -\xi_{e1}^{(q,p)} & -\xi_{e12}^{(q,p)} & 0 \\ \xi_{e12}^{(q,p)} & -\xi_{e1}^{(q,p)} & 0 \\ 0 & 0 & -\xi_{e2}^{(q,p)} \end{bmatrix}, \quad (3b)$$

$$3^\circ(C_{\infty v}) : \begin{bmatrix} \xi_{ep}^{(q)} \\ \xi_{mp}^{(q)} \end{bmatrix} = \begin{bmatrix} \xi_{e1}^{(q,p)} & \xi_{e12}^{(q,p)} & 0 \\ -\xi_{e12}^{(q,p)} & \xi_{e1}^{(q,p)} & 0 \\ 0 & 0 & \xi_{e2}^{(q,p)} \end{bmatrix}, \quad (3c)$$

$$4^\circ(D_{\infty h}) : \begin{bmatrix} \xi_{ep}^{(q)} \end{bmatrix} = \begin{bmatrix} \xi_{e1}^{(q,p)} & \xi_{e12}^{(q,p)} & 0 \\ -\xi_{e12}^{(q,p)} & \xi_{e1}^{(q,p)} & 0 \\ 0 & 0 & \xi_{e2}^{(q,p)} \end{bmatrix},$$

$$\begin{bmatrix} \xi_{mp}^{(q)} \end{bmatrix} = \begin{bmatrix} \xi_{e1}^{(q,p)} & -\xi_{e12}^{(q,p)} & 0 \\ \xi_{e12}^{(q,p)} & \xi_{e1}^{(q,p)} & 0 \\ 0 & 0 & \xi_{e2}^{(q,p)} \end{bmatrix}. \tag{3d}$$

It is understood that, strictly speaking, all the elements in (3) should be a function of the operating angular frequency which is suppressed here.

3. FIELD DISTRIBUTION

In Fig. 1, the excitation is provided by a plane EM wave, and TM_z and TE_z polarizations are considered simultaneously. The normally incident wave with respect to the coordinate system $O(\rho, \varphi, z)$ can be expressed as

$$\begin{bmatrix} E_z^{inc} \\ H_z^{inc} \end{bmatrix} = \begin{bmatrix} A_{TM} E_0 \\ A_{TE} H_0 \end{bmatrix} e^{ik\rho \cos(\varphi - \varphi_0)}, \tag{4a, 4b}$$

For TM_z polarization $A_{TM} = 1, A_{TE} = 0$, while for TE_z polarization $A_{TE} = 1, A_{TM} = 0$. In the coordinate system $O_M^{(q)}(\rho_M^{(q)}, \varphi_M^{(q)}, z_M^{(q)})$, the incident fields can be stated as

$$\begin{bmatrix} E_{zM}^{inc(q)} \\ H_{zM}^{inc(q)} \\ E_{\varphi M}^{inc(q)} \\ H_{\varphi M}^{inc(q)} \end{bmatrix} = \sum_{n=-\infty}^{\infty} i^n e^{in(\varphi_M^{(q)} - \varphi_0)} e^{ik\rho_q' \cos(\varphi_q' - \varphi_0)} \begin{bmatrix} \tilde{J}_{nM}^{(q)} \end{bmatrix} \begin{bmatrix} E_0 A_{TM} \\ H_0 A_{TE} \end{bmatrix}, \tag{5a}$$

where

$$\begin{bmatrix} \tilde{J}_{nM}^{(q)} \end{bmatrix} = \begin{bmatrix} J_{nM}^{(q)} & 0 \\ 0 & iJ_{nM}^{(q)}/\eta \\ 0 & J_{nM}^{(q)'} \\ iJ_{nM}^{(q)'}/\eta & 0 \end{bmatrix}, \tag{5b}$$

and $J_{nM}^{(q)} = J_n(k\rho_M^{(q)})$, $J_{nM}^{(q)'} = \left. \frac{\partial J_n(x)}{\partial x} \right|_{x=k\rho_M^{(q)}}$, $J_n(\cdot)$ is the n th-order Bessel function of the first kind.

Since the cross-polarization can be expected for every materials featuring bianisotropy, the scattered fields must have both TM_z and TE_z components owing to the existence of the multiple bianisotropic cylinders. So the scattered fields of the tangential components are expressed as

$$\begin{bmatrix} E_{zM}^{s(q)} \\ H_{zM}^{s(q)} \\ E_{\varphi M}^{s(q)} \\ H_{\varphi M}^{s(q)} \end{bmatrix} = \sum_{n=-\infty}^{\infty} e^{in\varphi_M^{(q)}} \left[\tilde{H}_{nM}^{(q)} \right] \begin{bmatrix} a_{nM}^{(q)} \\ b_{nM}^{(q)} \end{bmatrix}, \quad (6)$$

where $H_{nM}^{(q)} = H_n^{(2)}(k\rho_M^{(q)})$, $H_{nM}^{(q)'} = \frac{\partial H_n^{(2)}(x)}{\partial x} \Big|_{x=k\rho_M^{(q)}}$, $H_n^{(2)}(\cdot)$ is the n th Hankel function of the second kind and $a(b)_{nM}^{(q)}$ are the unknown coefficients determined from the boundary conditions.

Based on the gyrotropic form of the four constitutive tensors shown in (2), the tangential field components in the p th layer of the q th cylinder with respect to $O_1^{(q)}(\rho_1^{(q)}, \varphi_1^{(q)}, z_1^{(q)})$ can be written as

$$E_{zp}^{(q)} = \sum_{\pm} E_{zp\pm}^{(q)}, \quad H_{zp}^{(q)} = \sum_{\pm} H_{zp\pm}^{(q)}, \quad E_{\varphi p}^{(q)} = \sum_{\pm} E_{\varphi p\pm}^{(q)}, \quad H_{\varphi p}^{(q)} = \sum_{\pm} H_{\varphi p\pm}^{(q)}, \quad (7a)$$

and

$$\begin{bmatrix} E_{zp\pm}^{(q)} \\ H_{zp\pm}^{(q)} \\ E_{\varphi p\pm}^{(q)} \\ H_{\varphi p\pm}^{(q)} \end{bmatrix} = \sum_{n=-\infty}^{\infty} \begin{bmatrix} X_{1p\pm}^{(q)} & X_{2p\pm}^{(q)} \\ X_{3p\pm}^{(q)} & X_{4p\pm}^{(q)} \\ X_{5p\pm}^{(q)} & X_{6p\pm}^{(q)} \\ X_{7p\pm}^{(q)} & X_{8p\pm}^{(q)} \end{bmatrix} \begin{bmatrix} D_{1np\pm}^{(q)} \\ D_{2np\pm}^{(q)} \end{bmatrix} e^{in\varphi_1^{(q)}}, \quad (7b)$$

where $X_{sp\pm}^{(q)} (s = 1, \dots, 8)$ are presented in APPENDIX 1, and $D_{1np\pm}^{(q)}$ and $D_{2np\pm}^{(q)}$ are unknown mode expanding coefficients. Especially, for a bianisotropic core ($p = 1$), we should have $D_{2n1\pm}^{(q)} = 0$ by taking account of the singularity of the Neumann function at the origin. So, enforcing the boundary conditions of tangential continuous electric and magnetic fields at $\rho_1^{(q)} = R_1^{(q)}$, we have

$$\begin{bmatrix} x_{11}^{(q)} \\ \tilde{d}_1^{(q)} \end{bmatrix} = \begin{bmatrix} x_{12}^{(q)} \\ \tilde{d}_2^{(q)} \end{bmatrix}, \quad (8a)$$

and

$$\begin{aligned}
 \left[x_{11}^{(q)} \right] &= \begin{bmatrix} X_{11+}^{(q)} & X_{11-}^{(q)} & 0 & 0 \\ X_{31+}^{(q)} & X_{31-}^{(q)} & 0 & 0 \\ X_{51+}^{(q)} & X_{51-}^{(q)} & 0 & 0 \\ X_{71+}^{(q)} & X_{71-}^{(q)} & 0 & 0 \end{bmatrix}, \\
 \left[x_{12}^{(q)} \right] &= \begin{bmatrix} X_{12+}^{(q)} & X_{22+}^{(q)} & X_{12-}^{(q)} & X_{22-}^{(q)} \\ X_{32+}^{(q)} & X_{42+}^{(q)} & X_{32-}^{(q)} & X_{42-}^{(q)} \\ X_{52+}^{(q)} & X_{62+}^{(q)} & X_{52-}^{(q)} & X_{62-}^{(q)} \\ X_{72+}^{(q)} & X_{82+}^{(q)} & X_{72-}^{(q)} & X_{82-}^{(q)} \end{bmatrix}, \\
 \left[\tilde{d}_1^{(q)} \right] &= \left[D_{1n1+}^{(q)} \quad D_{1n1-}^{(q)} \quad 0 \quad 0 \right]^T, \\
 \left[\tilde{d}_2^{(q)} \right] &= \left[D_{1n2+}^{(q)} \quad D_{2n2+}^{(q)} \quad D_{1n2-}^{(q)} \quad D_{2n2-}^{(q)} \right]^T. \tag{8b}
 \end{aligned}$$

where the superscript T denotes the transpose of matrix. For an impedance core ($p = 1$), (8a, b) are turned into

$$\begin{bmatrix} Y_{12+}^{(q)} & Y_{22+}^{(q)} & Y_{12-}^{(q)} & Y_{22-}^{(q)} \\ Y_{32+}^{(q)} & Y_{42+}^{(q)} & Y_{32-}^{(q)} & Y_{42-}^{(q)} \\ 0 & 0 & 0 & 0 \\ 0 & 0 & 0 & 0 \end{bmatrix} \left[\tilde{d}_2^{(q)} \right] = [0], \tag{9a}$$

where

$$\begin{aligned}
 Y_{12\pm}^{(q)} &= X_{12\pm}^{(q)} + \eta_z^{(q)} X_{72\pm}^{(q)}, & Y_{22\pm}^{(q)} &= X_{22\pm}^{(q)} + \eta_z^{(q)} X_{82\pm}^{(q)}, \\
 Y_{32\pm}^{(q)} &= X_{52\pm}^{(q)} - \eta_\varphi^{(q)} X_{32\pm}^{(q)}, & Y_{42\pm}^{(q)} &= X_{62\pm}^{(q)} - \eta_\varphi^{(q)} X_{42\pm}^{(q)}. \tag{9b}
 \end{aligned}$$

Here $\eta_z^{(q)}$ and $\eta_\varphi^{(q)}$ are the surface impedances at $\rho_1^{(q)} = R_1^{(q)}$. The boundary conditions for the tangential components of the electric and magnetic fields at $\rho_p^{(q)} = R_p^{(q)}$ and $\rho_1^{(q)} = R_1^{(q)}$ ($2 \leq p \leq M$) are to be enforced. This requires that the fields (7) must be translated into the coordinate system $O_p^{(q)}(\rho_p^{(q)}, \varphi_p^{(q)}, z_p^{(q)})$ using the translational addition theorem (TATM) for cylindrical wave functions, i.e.,

$$\begin{aligned}
 Z_n \left(\sqrt{S_{p\pm}^{(q)}} \rho_1^{(q)} \right) e^{in\varphi_1^{(q)}} &= \sum_{m=-\infty}^{+\infty} Z_{m-n} \left(\sqrt{S_{p\pm}^{(q)}} \rho_p^{(q)} \right) \\
 &\cdot J_m \left(\sqrt{S_{p\pm}^{(q)}} d_{p1}^{(q)} \right) e^{i[m\varphi_p^{(q)} - (m-n)\varphi_{p1}^{(q)}]}, \tag{10}
 \end{aligned}$$

where $\varphi_{p1}^{(q)}$ is the angle between the line $O_p^{(q)}O_1^{(q)}$ and the x -axis. Furthermore, (7a, b) become

$$\begin{bmatrix} E_{zp\pm}^{(q)} \\ H_{zp\pm}^{(q)} \\ E_{\varphi p\pm}^{(q)} \\ H_{\varphi p\pm}^{(q)} \end{bmatrix} = \sum_{m=-\infty}^{+\infty} \sum_{n=-\infty}^{\infty} \begin{bmatrix} \tilde{X}_{1p\pm}^{(q)} & \tilde{X}_{2p\pm}^{(q)} \\ \tilde{X}_{3p\pm}^{(q)} & \tilde{X}_{4p\pm}^{(q)} \\ \tilde{X}_{5p\pm}^{(q)} & \tilde{X}_{6p\pm}^{(q)} \\ \tilde{X}_{7p\pm}^{(q)} & \tilde{X}_{8p\pm}^{(q)} \end{bmatrix} \begin{bmatrix} D_{1np\pm}^{(q)} \\ D_{2np\pm}^{(q)} \end{bmatrix} e^{im\varphi_p^{(q)}}, \quad (11a)$$

and

$$\begin{aligned} \tilde{X}_{sp\pm}^{(q)} &= e^{-i(m-n)\varphi_{p1}^{(q)}} X_{sp\pm}^{(q)} \Big|_{(J,N) \rightarrow (\tilde{J},\tilde{N}); 1 \rightarrow p}, \\ \tilde{J}_{mnp\pm}^{(q,l)} &= J_m \left(\sqrt{S_{p\pm}^{(q)}} \rho_p^{(q)} \right) J_{m-n} \left(\sqrt{S_{p\pm}^{(q)}} d_{p1}^{(q)} \right), \\ \tilde{N}_{mnp\pm}^{(q,l)} &= J_m \left(\sqrt{S_{p\pm}^{(q)}} \rho_p^{(q)} \right) N_{m-n} \left(\sqrt{S_{p\pm}^{(q)}} d_{p1}^{(q)} \right). \end{aligned} \quad (11b)$$

Thus, using the boundary conditions of continuous tangential electric and magnetic fields at $\rho_p^{(q)} = R_p^{(q)}$ ($2 \leq p \leq M-1$), we find

$$\sum_{n=-\infty}^{+\infty} \begin{bmatrix} x_{1p}^{(q)} \\ \tilde{d}_p^{(q)} \end{bmatrix} = \sum_{n=-\infty}^{+\infty} \begin{bmatrix} x_{1p+1}^{(q)} \\ \tilde{d}_{p+1}^{(q)} \end{bmatrix}, \quad (12)$$

In order to exploit the boundary conditions on the external surface $\rho_M^{(q)} = R_M^{(q)}$, the TATM shown in APPENDIX 2 for the Hankel functions must be employed, and the boundary conditions for the electric and magnetic fields results in

$$\begin{aligned} \sum_{n=-\infty}^{+\infty} \begin{bmatrix} x_{1M}^{(q)} \\ \tilde{d}_M^{(q)} \end{bmatrix} &= i^m e^{-im\varphi_0} e^{ik\rho'_q \cos(\varphi'_q - \varphi_0)} \begin{bmatrix} \tilde{J}_{mM}^{(q)} \\ \tilde{H}_{mM}^{(q)} \end{bmatrix} \begin{bmatrix} E_0 A_{TM} \\ H_0 A_{TE} \end{bmatrix} \\ &+ \begin{bmatrix} \tilde{H}_{mM}^{(q)} \\ \tilde{J}_{mM}^{(q)} \end{bmatrix} \begin{bmatrix} a_{mM}^{(q)} \\ b_{mM}^{(q)} \end{bmatrix} + \begin{bmatrix} \tilde{J}_{mM}^{(q)} \\ \tilde{H}_{mM}^{(q)} \end{bmatrix} \\ &\sum_{\substack{g=1 \\ g \neq q}}^N \sum_{n=-\infty}^{+\infty} H_{m-n}^{(2)}(kD_{qg}) e^{-i(m-n)\varphi'_{qg}} \begin{bmatrix} a_{nM}^{(g)} \\ b_{nM}^{(g)} \end{bmatrix} \end{aligned} \quad (13)$$

in which the last terms of the series summations at the right handside is the mutual coupling between q and g , $g = 1, 2, \dots, N (q \neq g)$

cylinders, and it should be noted that the above system equations (8) or (9), (12) and (13) are solved for each m independently. To find a numerical solution of the $a(b)_{nM}^{(q)} (q = 1, \dots, N)$, all the system equations must be truncated to a finite size. Physical intuition suggests that the truncation $N_0(m, n = -N_0, \dots, N_0)$ depends mainly on the electric size $\max \{k_0 R_M^{(q)}\}$, and N_0 becomes not very large for above electrically non-large case. Including the terms $(2N_0 + 1)$ in the series summations above leads to $L = 4(2N_0 + 1)$ equations in (8) or (9), (12) and (13), respectively. So the system equations for the unknown coefficients $a(b)_{nM}^{(q)}$ are stated as:

$$\begin{aligned}
 & \left[X_{MM}^{(q)} \right]_{L \times L} \left[X^{(q)} \right]_{L \times L}^{-1} \left[X_{11}^{(q)} \right]_{L \times L} \left[D_1^{(q)} \right]_{L \times 1} - \left[\tilde{H}_{mM}^{(q)} \right] \begin{bmatrix} a_{mM}^{(q)} \\ b_{mM}^{(q)} \end{bmatrix} \\
 & - \left[\tilde{J}_{mM}^{(q)} \right] \sum_{\substack{g=1 \\ g \neq q}}^N \sum_{n=-\infty}^{+\infty} H_{m-n}^{(2)}(kD_{gg}) e^{-i(m-n)\varphi_{gg}} \begin{bmatrix} a_{nM}^{(g)} \\ b_{nM}^{(g)} \end{bmatrix} \\
 & = i^m e^{-im\varphi_0} e^{ik\rho'_q \cos(\varphi'_q - \varphi_0)} \begin{bmatrix} \tilde{J}_{mM}^{(q)} \\ H_{0ATE} \end{bmatrix} \begin{bmatrix} E_0 A_{TM} \\ H_0 A_{TE} \end{bmatrix} \quad (14)
 \end{aligned}$$

in which all the matrices are defined in APPENDIX 3.

Alternatively, for N cylinder we can obtain N system equations taking a similar form as (14) ($q = 1, \dots, N$) for all the unknown coefficients $a(b)_{nM}^{(q)}$ and the numerical solution is feasible. However, most of the computer time is consumed by the system matrix inversion and not for matrix filling. Therefore, for a large number of N a reduction in the CPU time for the matrix inversion can be achieved using the fast iterative scattering technique as shown as in [17, 41, 42]. On the other hand, for electrically large cylinders, N_0 should be chosen to be very large, and under such circumstance, the asymptotic technique of geometric optics must be adopted [5].

Furthermore, the far scattered field can then be computed after using the large argument approximation of Hankel function, and the corresponding formulations for determining of the co- and cross-polarized scattering cross sections ($\sigma^{co(cross)}$), or the echo width are presented in [28] and [31], respectively. However, it should be pointed out that the definitions of σ^{cross} in [31] is different from that in [28].

On the other hand, it is well known that, according to the principle of equal volume model, the scattering of an electromagnetic wave

from two-dimensional objects of arbitrary cross sections can be approximately modeled by a number of circular cylinders with the same constitutive relations [42]. Therefore, the above planar array can be exploited to model the scattering of various two-dimensional complex bianisotropic objects described by the constitutive relations (1a, b) and (2). Based on the scattering model shown in [8], Table 1 shows the modeling arrangements of some bianisotropic cylinders, and such arrangements are proven to be accurate enough for predicting the scattering characteristics of bianisotropic objects for a plane wave as well as a beam wave incidence of TM_z or TE_z polarization.

In Table 1, the modeling cylinders' radii can be chosen to be ($p = 1$) :

for case (a),

$$R_1^{(q)} = \{0.2500\lambda, 0.0126\lambda, 0.0252\lambda, 0.0518\lambda, 0.0252\lambda, 0.0126\lambda, \dots, \\ 0.0126\lambda, 0.0252\lambda, 0.0518\lambda, 0.0252\lambda, 0.0126\lambda, q=1, 2, \dots, 21, \\ \sum_{q=1}^{21} V_q = 0.25\lambda^2\}$$

for case (b),

$$R_1^{(q)} = \{0.2500\lambda, 0.0126\lambda, 0.0252\lambda, 0.0518\lambda, 0.0252\lambda, 0.0126\lambda, \\ 0.0126\lambda, 0.0252\lambda, 0.0518\lambda, 0.0252\lambda, 0.0126\lambda, 0.0126\lambda, \\ 0.0252\lambda, 0.0518\lambda, 0.0252\lambda, 0.0126\lambda, \sum_{q=1}^{16} V_q = 0.2366\lambda^2\}.$$

for cases (c) and (d),

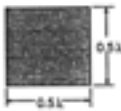
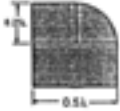


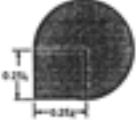

$$R_1^{(q)} = \{0.2500\lambda, 0.0126\lambda, 0.0252\lambda, 0.0518\lambda, 0.0252\lambda, 0.0126\lambda, \\ 0.0126\lambda, 0.0252\lambda, 0.0518\lambda, 0.0252\lambda, 0.0126\lambda, \\ \sum_{q=1}^{11} V_q = 0.2232\lambda^2\}.$$

for case (e),

$$R_1^{(q)} = \{0.2500\lambda, 0.0126\lambda, 0.0252\lambda, 0.0518\lambda, 0.0252\lambda, 0.0126\lambda, \sum_{q=1}^6 V_q = 0.2091\lambda^2\}.$$

Here $\sum_{q=1}^N V_q$ is the total volume of the modeling cylinders per length.

Table 1. The Modeling of five kinds of (in)homogeneous bianisotropic cylinders.

real cross-section:				
				
(a)	(b)	(c)	(d)	(e)
modeling arrangement:				
				
modeling cylinder number:				
21	16	11	11	6

4. NUMERICAL RESULTS AND DISCUSSIONS

Some computer codes have been developed for calculating the co- and the cross-polarized echo widths of various multiple bianisotropic planar arrays, and also the (an)isotropic case is applicable when the magneto-electric cross-coupling tensors $[\xi_{ep,mp}^{(q)}]$ are chosen to be very small. For practical consideration, the permittivity ϵ_b and permeability μ_b of the isotropic medium are assumed to be $\epsilon_b = \epsilon_0$ and $\mu_b = \mu_0$ in

the following numerical examples, while the losses of the bianisotropic cylinders are not taken into account in order that the attenuation by the cylinders can not mask the constitutive parameter effects. Because the literature appears to contain very little numerical data for scattering by inhomogeneous bianisotropic objects, we have not found any theoretical or measurement results for our models in the literature for comparison. However, the validity of our programs, including the accuracy and convergence rate, can be checked indirectly by comparing our results with those shown in [2, 4, 42]. For example, the scattered far field of the most simple case of two parallel identically isotropic circular cylinders has been reproduced at first using the above model case $p = 3$, $q = 2$. The truncation term number is $N_0 = 10$ and the related geometrical parameters are the same as in [42].

In Fig. 2, we let $[\xi_{ep}^{(q)}] = -[\xi_{mp}^{(q)}] = -i10^{-5}\sqrt{\mu_0\varepsilon_0\bar{I}}$ as an approach to zero, so their effects can be neglected. Obviously, the results shown in Fig. 2 are in excellent agreement with the corresponding results presented in [42].

Fig. 3 shows the co- and cross-polarized echo widths of two-layer, four eccentric bianisotropic cylinders ($p = 2$, $q = 1, 2, 3, 4$) corresponding to two different constitutive models, and the inner region ($p = 1$) for each of the four cylinders is assumed to be of ordinary gyroelectric material. Also, the convergence behavior of the above summations with increasing number N_0 has been checked for case (a), and some values of the $\sigma^{co(cross)}$ are listed in Table 2. Evidently, at least six-digit accuracy can be achieved for $N_0 \geq 10$.

In Fig. 3, only the TM_z -wave incidence is considered, and two different constitutive models of the UBM are demonstrated corresponding to the magnetic groups D_∞ and $D_{\infty h}$, respectively [36]. It is known that these UBM can be realized artificially by embedding the right-handed (RH) or the left-handed (LH) helical elements into a homogeneous medium in some special ways. Since $[\xi_{e2,m2}^{(q)}]$ are introduced here, the cross-polarized field component σ^{cross} can be expected as shown above. For such two UB models, both σ^{co} and σ^{cross} exhibit a very different behavior, except that in the forward range $\varphi = \varphi_0 + 180^\circ$ for the co-polarized component. It is obvious that, generally speaking, the de-polarized effect for case (a) is stronger than that of case (b) under the above circumstances. However, it must be emphasized that $\sigma^{co(cross)}$ is a function of many factors: all the elements of the four constitutive tensors, the geometrical parameters of the multiple cylin-

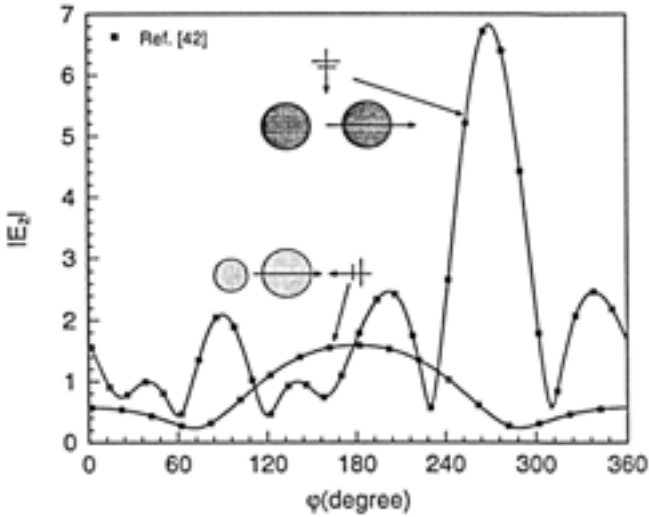


Figure 2. The scattered far fields of two parallel isotropic cylinders.

$$\varphi_3^{(1)} = 0^\circ, \quad \varphi_3^{(2)} = 180^\circ, \quad [\mu_p^{(q)}] = \mu_0 \bar{I}, \quad [\xi_{ep}^{(q)}] = -[\xi_{mp}^{(q)}] = -i10^{-5} \sqrt{\mu_0 \varepsilon_0} \bar{I}, \quad d_{21}^{(q)} = d_{31}^{(q)} = 0.0,$$

$$(a) \quad \varphi_0 = 90^\circ, \quad [\varepsilon_p^{(q)}] = 4.0 \varepsilon_0 \bar{I}, \quad R_3^{(q)} = 0.2\lambda, \quad R_{1,2}^{(q)} < R_3^{(q)}, \quad D_{12} = 0.8\lambda.$$

$$(b) \quad \varphi_0 = 0^\circ, \quad [\varepsilon_p^{(q)}] = 2.0 \varepsilon_0 \bar{I}, \quad R_3^{(1)} = 0.2\lambda, \quad R_3^{(2)} = 0.1\lambda, \quad R_{1,2}^{(q)} < R_3^{(q)}, \quad D_{12} = 0.4\lambda.$$

ders, the incident wave frequency, direction and polarization state, et al.. The appearance of the different effects shown above depends on the combination of all these factors. In addition, various numerical tests prove that,

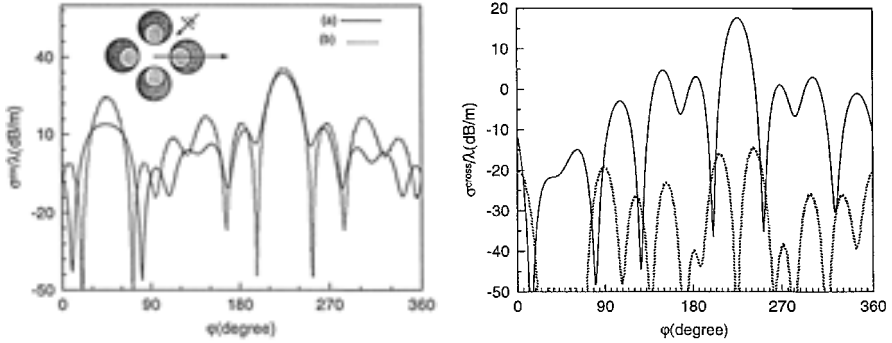


Figure 3. $\sigma^{co(cross)}$ versus φ for two-layer, four composite eccentric UB cylinders. $f = 10$ GHz, $\varphi_0 = 45^\circ$, $k_0 R_1^{(q)} = 1.0$, $k_0 R_2^{(q)} = 1.5$, $N_0 = 10$, $k_0 \rho'_q = 4.0$, $[\xi_{e1}^{(q)}] = -[\xi_{m1}^{(q)}] = -i10^{-6} \sqrt{\mu_0 \varepsilon_0} \bar{I}$, $\varphi_{21}^{(q)} = 180^\circ, 270^\circ, 0^\circ, 90^\circ$, $q = 1, 2, 3, 4$, $\varepsilon_1^{(q,1)} = 2.54\varepsilon_0$, $\varepsilon_2^{(q,1)} = 2.0\varepsilon_0$, $\varepsilon_{12}^{(q,1)} = 0.5\varepsilon_0$, $[\mu_1^{(q)}] = \mu_0 \bar{I}$, $\varepsilon_1^{(q,2)} = 4.0\varepsilon_0$, $\varepsilon_2^{(q,2)} = 4.5\varepsilon_0$, $\mu_1^{(q,2)} = \mu_0$, $\mu_2^{(q,2)} = 1.5\mu_0$,

(a) $[\xi_{e2}^{(q)}] = -[\xi_{m2}^{(q)}] = -i\sqrt{\mu_0 \varepsilon_0} \begin{bmatrix} 0.5 & 0 & 0 \\ 0 & 0.5 & 0 \\ 0 & 0 & 0.8 \end{bmatrix}$ (solid line).

(b) The parameters are the same as (a), except that

$[\xi_{e2}^{(q)}] = -[\xi_{m2}^{(q)}] = \sqrt{\mu_0 \varepsilon_0} \begin{bmatrix} 0 & 0.5 & 0 \\ -0.5 & 0 & 0 \\ 0 & 0 & 0 \end{bmatrix}$ (dotted line).

Table 2. Convergence tests for $\sigma^{co(cross)}/\lambda$ (dB/m) with increasing N_0 ($\varphi = 180^\circ$).

N_0	σ^{co}/λ	σ^{cross}/λ
2	9.031404	-0.300889
3	9.264615	2.636485
4	9.190021	2.204315
5	9.188913	2.222466
6	9.189195	2.221129
7	9.189189	2.221049
8	9.189191	2.221022
9	9.189192	2.221014
10	9.189192	2.221011
11	9.189192	2.221010

for TM_z incidence,

$$E_z \left(\pm \left[\xi_{ep}^{(q)} \right], \pm \left[\xi_{mp}^{(q)} \right] \right) = E_z \left(\mp \left[\xi_{ep}^{(q)} \right], \mp \left[\xi_{mp}^{(q)} \right] \right), \quad (15a)$$

$$H_z \left(\pm \left[\xi_{ep}^{(q)} \right], \pm \left[\xi_{mp}^{(q)} \right] \right) = -H_z \left(\mp \left[\xi_{ep}^{(q)} \right], \mp \left[\xi_{mp}^{(q)} \right] \right), \quad (15b)$$

for TE_z incidence,

$$E_z \left(\pm \left[\xi_{ep}^{(q)} \right], \pm \left[\xi_{mp}^{(q)} \right] \right) = -E_z \left(\mp \left[\xi_{ep}^{(q)} \right], \mp \left[\xi_{mp}^{(q)} \right] \right), \quad (15c)$$

$$H_z \left(\pm \left[\xi_{ep}^{(q)} \right], \pm \left[\xi_{mp}^{(q)} \right] \right) = H_z \left(\mp \left[\xi_{ep}^{(q)} \right], \mp \left[\xi_{mp}^{(q)} \right] \right), \quad (15d)$$

for $TM(E)_z$ incidence,

$$\sigma^{co(cross)} \left(\pm \left[\xi_{ep}^{(q)} \right], \pm \left[\xi_{mp}^{(q)} \right] \right) = \sigma^{co(cross)} \left(\mp \left[\xi_{ep}^{(q)} \right], \mp \left[\xi_{mp}^{(q)} \right] \right). \quad (15e)$$

Fig. 4 shows the $\sigma^{co(cross)}$ of two-layer, four identical touching gyrotropic bianisotropic (GB) cylinders corresponding to the magnetic groups $C_{\infty v}$, D_{∞} and $D_{\infty h}$ [36], respectively ($p = 1, 2$, $q = 1, 2, 3, 4$), while the inner region ($p = 1$) for each of the four cylinders is supposed to be a ferrite biased by a dc magnetic field. The particular interest here is the combined effect of both gyrotropy and bianisotropy on the co- and cross-polarized echo widths.

In Fig. 4, the touching bianisotropic cylinders are assumed to be the non-magnetic with $\left[\mu_2^{(q)} \right] = \mu_0 \bar{I}$ ($q = 1, 2, 3, 4$), while the permittivity tensor $\left[\varepsilon_2^{(q)} \right]$ and the magnetoelectric-coupling tensors $\left[\xi_{e2,m2}^{(q)} \right]$ are all in a gyrotropic form, respectively [39, 40]. In addition, it should be pointed out that the magnitude of each element of $\left[\xi_{e2,m2}^{(q)} \right]$ is in a physically reasonable confinement. Comparing case (a) with (b) or (c), it is obvious that the co-polarized component σ^{co} changes in an approximately similar way for TM_z (or TE_z) wave incidence, and it reaches the maximum in the forward direction $\varphi = 225^\circ$. However, the de-polarized component σ^{cross} is strongly governed by both $\left[\xi_{e2}^{(q)} \right]$ and $\left[\xi_{m2}^{(q)} \right]$, and significant cross-polarized contribution is expected for case (c) even for normal incidence. It is also predicated that such de-polarized effect can be further enhanced for oblique incidence. Naturally, the relations (15a)–(15e) hold true for these GB models.

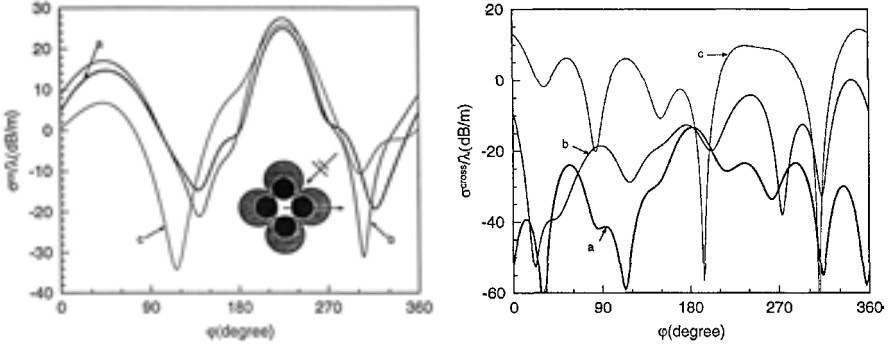


Figure 4. $\sigma^{co(cross)}$ versus φ for two-layer, four touching composite eccentric GB cylinders. $f = 10$ GHz, $\varphi_0 = 45^\circ$, $k_0 R_1^{(q)} = 1.0$, $k_0 R_2^{(q)} = 1.5$, $k_0 \rho'_q = 2.12$, $[\xi_{e1}^{(q)}] = -[\xi_{m1}^{(q)}] = -i10^{-6} \sqrt{\mu_0 \varepsilon_0 \bar{I}}$, $\varphi_{21}^{(q)} = 180^\circ$, 270° , 0° , 90° , $q = 1, 2, 3, 4$, $N_0 = 10$, $[\varepsilon_1^{(q)}] = 12.6 \varepsilon_0 \bar{I}$, $M_s^{(q)} \mu_0 = 0.275 T$, $\omega_0^{(q)} / \omega_m^{(q)} = 0.3$, $\mu_2^{(q,1)} = \mu_0$, $\mu_1^{(q,1)} = \mu_0 \omega_0^{(q)} \omega_m^{(q)} / [\omega_0^{(q)2} - \omega^2]$, $\mu_{12}^{(q,1)} = -\mu_0 \omega \omega_m^{(q)} / [\omega_0^{(q)2} - \omega^2]$, $\varepsilon_1^{(q,2)} = 4.0 \varepsilon_0$, $\varepsilon_2^{(q,2)} = 4.5 \varepsilon_0$, $\varepsilon_{12}^{(q,2)} = 0.5 \varepsilon_0$, $\omega_m^{(q)} = 2.21 \times 10^5 M_s^{(q)}$, $[\mu_2^{(q)}] = \mu_0 \bar{I}$, $\omega_0^{(q)} = 2.21 \times 10^5 H_0^{(q)}$, $H_0^{(q)}$ is the magnitude of the internal dc bias field,

$$(a) \left[\xi_{e2}^{(q)} \right] = - \left[\xi_{m2}^{(q)} \right] = \sqrt{\mu_0 \varepsilon_0} \left[C_2^{(q)} \right], \quad \left[C_2^{(q)} \right] = \begin{bmatrix} -i0.5 & 0.6 & 0 \\ -0.6 & -i0.5 & 0 \\ 0 & 0 & -i0.8 \end{bmatrix}.$$

$$(b) \left[\xi_{e2}^{(q)} \right] = \left[\xi_{m2}^{(q)} \right] = \sqrt{\mu_0 \varepsilon_0} \left[C_2^{(q)} \right].$$

$$(c) \left[\xi_{e2}^{(q)} \right] = \sqrt{\mu_0 \varepsilon_0} \begin{bmatrix} i0.5 & 0.6 & 0 \\ -0.6 & i0.5 & 0 \\ 0 & 0 & i0.8 \end{bmatrix}, \quad \left[\xi_{m2}^{(q)} \right] = \sqrt{\mu_0 \varepsilon_0} \begin{bmatrix} i0.5 & -0.6 & 0 \\ 0.6 & i0.5 & 0 \\ 0 & 0 & i0.8 \end{bmatrix}.$$

Furthermore, the co- and cross-polarized scattering echo widths $\sigma^{co(cross)}$ of an inhomogeneous bianisotropic square cylinder is depicted in Fig. 5, which is successfully modeled by using one ferrite circular cylinder combined with 20 UB circular cylinders of different radii and same constitutive parameters ($p = 1$). The arrangement of 21 circular cylinders is shown in Table 1, and the computed results for the isotropic square cylinder is in a good agreement with that obtained by a moment method [42].

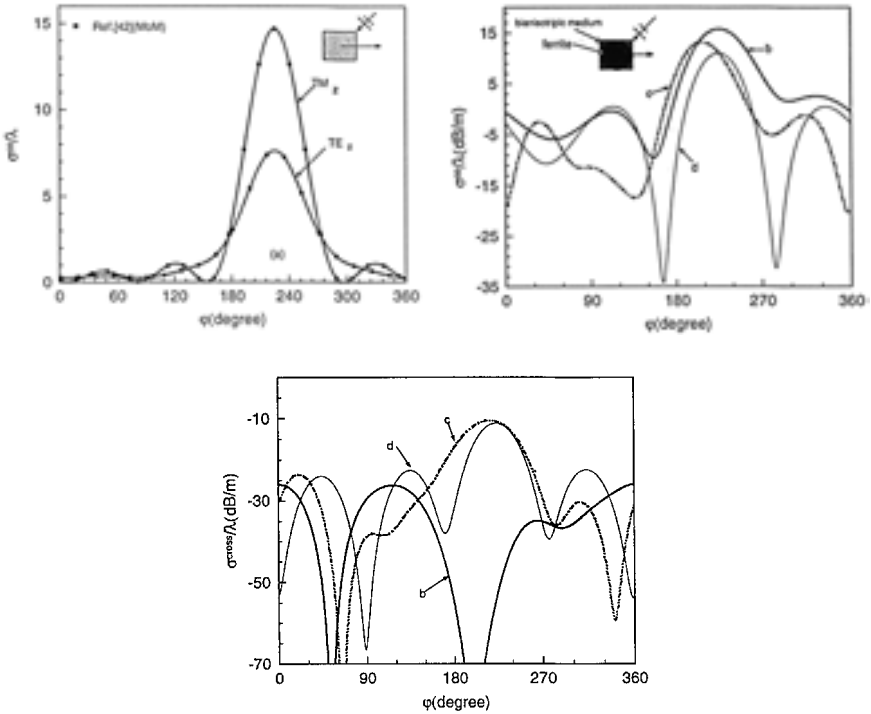


Figure 5. $\sigma^{co(cross)}$ versus φ for a ferrite and UB composite square cylinder. $f = 10$ GHz, $k_0d = 3.1416$, $\varphi_0 = 45^\circ$,

- (a) $[\varepsilon_1^{(q)}] = 4.0\varepsilon_0\bar{\bar{I}}$, $[\mu_1^{(q)}] = \mu_0\bar{\bar{I}}$, $[\xi_{e1}^{(q)}] = [\xi_{m1}^{(q)}] = -i10^{-6}\sqrt{\mu_0\varepsilon_0}\bar{\bar{I}}$,
 $q = 1, 2, \dots, 21$.
- (b) $[\varepsilon_1^{(1)}] = 12.6\varepsilon_0\bar{\bar{I}}$, $M_s^{(1)}\mu_0 = 0.275T$, $\omega_m^{(1)} = 2.21 \times 10^5 M_s^{(1)}$, $\mu_2^{(1,1)} = \mu_0$,
 $\mu_1^{(1,1)} = \mu_0\omega_0^{(1)}\omega_m^{(1)} / [\omega_0^{(1)2} - \omega^2]$, $\mu_{12}^{(1,1)} = -\mu_0\omega\omega_m^{(1)} / [\omega_0^{(1)2} - \omega^2]$,
 $\varepsilon_1^{(q,1)} = 4.0\varepsilon_0$, $\varepsilon_2^{(q,1)} = 4.5\varepsilon_0$, $\mu_1^{(q,1)} = 1.0\mu_0$, $\mu_2^{(q,1)} = 1.5\mu_0$, $q = 2, \dots, 21$,
 $\xi_{e1}^{(q,1)} = -\xi_{m1}^{(q,1)} = -i0.5\sqrt{\mu_0\varepsilon_0}$, $\xi_{e2}^{(q,1)} = -\xi_{m2}^{(q,1)} = -i0.8\sqrt{\mu_0\varepsilon_0}$,
 $\omega_0^{(1)}/\omega_m^{(1)} = 0.3$.
- (c) The par ameters are the same as (b), except that $\omega_0^{(1)}/\omega_m^{(1)} = 1.5$.
- (d) The par ameters are the same as (c), except that $\omega_0^{(1)}/\omega_m^{(1)} = 2.5$.

In Figs. 5(b)–(d), only the plane TM_z -wave incidence is demonstrated ($\varphi_0 = 45^\circ$), and such an inhomogeneous bianisotropic square cylinder is assumed to be the same geometrical size ($0.5 \times 0.5\lambda^2$) as in case (a). With respect to the coordinate system of XOY, the locations of the 21 modeling cylinders are determined by:

$$(\rho'_q, \varphi'_q) = (0, 0^\circ), (0.007878, 22.3233^\circ), (0.008256, 30.2203^\circ), (0.009053, 45^\circ), (0.008256, 59.7796^\circ), (0.007878, 67.6766^\circ), \dots, (0.009053, 135^\circ), \dots, (0.009053, 225^\circ), \dots, (0.009053, 315^\circ).$$

It is apparent that for this special geometry the indirect modeling technique is efficient, flexible and has some advantages over the direct numerical method. The magnitude of σ^{co} in the forward range is decreased with the increasing of the bias field intensity $\omega_0^{(1)}/\omega_m^{(1)}$ from $0.3 \rightarrow 1.5 \rightarrow 2.5$, and conversely, σ^{cross} is increased. In some special direction, the de-polarized effect can disappear in the scattered field for case (b) or (c). So $\sigma^{co(cross)}$ can be effectively adjusted by varying the bias field intensity $\omega_0^{(1)}/\omega_m^{(1)}$.

Finally, Fig. 6 depicts the co- and cross-polarized scattered field characteristics of three kinds of irregular cylinders for TM_z -wave incidence, and they are all composites of ferrite and GB media. The geometrical shapes of the cross sections are the same as shown in Table 1(b), (c) and (d), respectively, and the radius of the central ferrite is $R_1^{(1)} = 0.25\lambda$ as above.

In Fig. 6, the bianisotropic cylinders are non-magnetic with $[\mu_1^{(q)}] = \mu_0 \bar{\bar{I}}$, and the permittivity tensor $[\varepsilon_1^{(q)}]$ as well as the magnetoelectric-coupling tensors $[\xi_{e1,m1}^{(q)}]$ are all in a gyrotropic form corresponding to the magnetic group $C_{\infty v}$ [36]. Based on the arrangement shown in Table 1 or in Figs. 5(b)–(d), such three irregular composite cylinders are modeled using 16 and 11 circular cylinders, respectively. The locations of the 11 modeling cylinders for case (c) are given by:

$$(\rho'_q, \varphi'_q) = (0, 0^\circ), (0.007878, 202.3233^\circ), (0.008256, 210.2203^\circ), (0.009053, 225^\circ), (0.008256, 239.7796^\circ), (0.007878, 247.6766^\circ), (0.007878, 292.3233^\circ), (0.008256, 300.2203^\circ), (0.009053, 315^\circ), (0.008256, 329.7796^\circ), (0.007878, 337.6766^\circ).$$

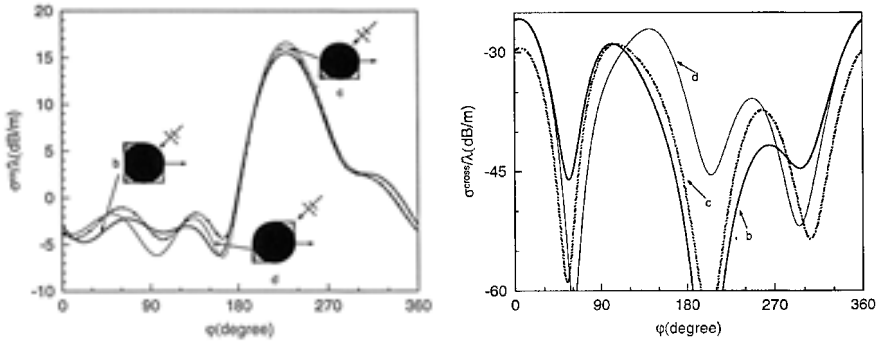


Figure 6. $\sigma^{co(cross)}$ versus φ for three irregular composite cylinders of the ferrite and GB medium. $f = 10 \text{ GHz}$, $k_0 d = 3.1416$, $\varphi_0 = 45^\circ$, $[\varepsilon_1^{(1)}] = 12.6\varepsilon_0 \bar{I}$, $M_s^{(1)} \mu_0 = 0.275T$, $\omega_m^{(1)} = 2.21 \times 10^5 M_s^{(1)}$, $\mu_2^{(1,1)} = \mu_0$, $\mu_1^{(1,1)} = \mu_0 \omega_0^{(1)} \omega_m^{(1)} / [\omega_0^{(1)2} - \omega^2]$, $\mu_{12}^{(1,1)} = -\mu_0 \omega \omega_m^{(1)} / [\omega_0^{(1)2} - \omega^2]$, $\omega_0^{(1)} / \omega_m^{(1)} = 0.3$, $\varepsilon_1^{(q,1)} = 4.0\varepsilon_0$, $\varepsilon_2^{(q,1)} = 4.5\varepsilon_0$, $\varepsilon_{12}^{(q,1)} = 0.5\varepsilon_0$, $[\mu_1^{(q)}] = \mu_0 \bar{I}$, $[\xi_{e1}^{(q)}] = -[\xi_{m1}^{(q)}] = \sqrt{\mu_0 \varepsilon_0} \begin{bmatrix} -i0.5 & 0.6 & 0 \\ -0.6 & -i0.5 & 0 \\ 0 & 0 & -i0.8 \end{bmatrix}$. (b): $q = 2, \dots, 16$. (c) (d): $q = 2, \dots, 11$.

While for case (d),

$$(\rho'_q, \varphi'_q) = (0, 0^\circ), (0.007878, 22.3233^\circ), (0.008256, 30.2203^\circ), (0.009053, 45^\circ), (0.008256, 59.7796^\circ), (0.007878, 67.6766^\circ), (0.007878, 202.3233^\circ), (0.008256, 210.2203^\circ), (0.009053, 225^\circ), (0.008256, 239.7796^\circ), (0.007878, 247.6766^\circ).$$

It is interesting to note that, the main differences in the magnitude of σ^{co} are nearly in the range of $\varphi \in [0^\circ, 180^\circ]$ and $[300^\circ, 360^\circ]$, and σ^{cross} changes in a similar way except that in some special direction φ .

Following the same way adopted above, similar conclusions can be drawn for the TE_z -wave incidence.

5. CONCLUSION

In this paper, the scattering from multiple composite bianisotropic cylinders has been investigated carefully, and our attention has been

paid to the combined effects of both geometrical and constitutive parameters of various bianisotropic cylindrical structures on the co- and cross-polarized scattering cross sections. It has been proven that the indirect modeling technique possesses the advantages of simplicity and efficiency under some circumstances. Actually, many bianisotropic cylindrical scatterers with complex cross-section, such as internal inhomogeneity, et al., can be modeled using the above given planar array in Fig. 1, and acceptable results for the scattering features of composites can be found. On the other hand, the present study can provide much insight into the electromagnetic scattering features of bianisotropic composites and their potential applications in microwave and millimeter wave regimes.

APPENDIX 1.

In (6),

$$\begin{aligned}
 X_{1p\pm}^{(q)} &= S_{p\pm}^{(q)} J_{np\pm}^{(q,1)}, \quad X_{2p\pm}^{(q)} = S_{p\pm}^{(q,1)} N_{np\pm}^{(q,1)}, \\
 X_{3p\pm}^{(q)} &= q_{p\pm}^{(q)} J_{np\pm}^{(q,1)}, \quad X_{4p\pm}^{(q)} = q_{p\pm}^{(q)} N_{np\pm}^{(q,1)}, \\
 X_{5p\pm}^{(q)} &= -M_{p\pm}^{(q)} J_{np\pm}^{(q,1)'} - \frac{inN_{p\pm}^{(q)}}{\rho_1^{(q)}} J_{np\pm}^{(q,1)}, \\
 X_{6p\pm}^{(q)} &= -M_{p\pm}^{(q)} N_{np\pm}^{(q,1)'} - \frac{inN_{p\pm}^{(q)}}{\rho_1^{(q)}} N_{np\pm}^{(q,1)}, \\
 X_{7p\pm}^{(q)} &= -X_{p\pm}^{(q)} J_{np\pm}^{(q,1)'} - \frac{inY_{p\pm}^{(q)}}{\rho_1^{(q)}} J_{np\pm}^{(q,1)}, \\
 X_{8p\pm}^{(q)} &= -X_{p\pm}^{(q)} N_{np\pm}^{(q,1)'} - \frac{inY_{p\pm}^{(q)}}{\rho_1^{(q)}} N_{np\pm}^{(q,1)},
 \end{aligned}$$

and

$$\begin{aligned}
 J_{np\pm}^{(q,l)} &= J_n \left(\sqrt{S_{p\pm}^{(q)}} \rho_l^{(q)} \right), \quad N_{np\pm}^{(q,l)} = N_n \left(\sqrt{S_{p\pm}^{(q)}} \rho_l^{(q)} \right), \\
 J_{np\pm}^{(q,l)'} &= J'_n \left(\sqrt{S_{p\pm}^{(q)}} \rho_l^{(q)} \right), \quad N_{np\pm}^{(q,l)'} = N'_n \left(\sqrt{S_{p\pm}^{(q)}} \rho_l^{(q)} \right), \quad l = 1, 2, \dots, M, \\
 M_{p\pm}^{(q)} &= \sqrt{S_{p\pm}^{(q)}} \left(A_{21p}^{(q)} S_{p\pm}^{(q)} + A_{41p}^{(q)} Q_{p\pm}^{(q)} \right), \quad N_{p\pm}^{(q)} = \left(A_{22p}^{(q)} S_{p\pm}^{(q)} + A_{42p}^{(q)} Q_{p\pm}^{(q)} \right),
 \end{aligned}$$

$$\begin{aligned}
X_{p\pm}^{(q)} &= \sqrt{S_{p\pm}^{(q)}} \left(A_{23p}^{(q)} S_{p\pm}^{(q)} + A_{43p}^{(q)} Q_{p\pm}^{(q)} \right), \quad Y_{p\pm}^{(q)} = \left(A_{24p}^{(q)} S_{p\pm}^{(q)} + A_{44p}^{(q)} Q_{p\pm}^{(q)} \right), \\
S_{p\pm}^{(q)} &= \frac{-\left(P_{1p}^{(q)} + P_{4p}^{(q)} \right) \pm \sqrt{\left(P_{1p}^{(q)} - P_{4p}^{(q)} \right)^2 - 4P_{2p}^{(q)} P_{3p}^{(q)}}}{2}, \\
Q_{p\pm}^{(q)} &= -i \frac{S_{p\pm}^{(q)} \left(S_{p\pm}^{(q)} + P_{1p}^{(q)} \right)}{P_{2p}^{(q)}}, \\
P_{1p}^{(q)} &= i\omega \frac{A_{21p}^{(q)} \varepsilon_2^{(q,p)} + A_{23p}^{(q)} \xi_{m2}^{(q,p)}}{\Delta_p^{(q)}}, \quad P_{2p}^{(q)} = -\omega \frac{A_{43p}^{(q)} \mu_2^{(q,p)} + A_{41p}^{(q)} \xi_{e2}^{(q,p)}}{\Delta_p^{(q)}}, \\
P_{3p}^{(q)} &= \omega \frac{A_{21p}^{(q)} \varepsilon_2^{(q,p)} + A_{23p}^{(q)} \xi_{m2}^{(q,p)}}{\Delta_p^{(q)}}, \quad P_{4p}^{(q,p)} = -i\omega \frac{A_{21p}^{(q,p)} \xi_{e2}^{(q,p)} + A_{23p}^{(q,p)} \mu_2^{(q,p)}}{\Delta_p^{(q)}}, \\
\Delta_p^{(q)} &= A_{21p}^{(q)} A_{43p}^{(q)} - A_{23p}^{(q)} A_{41p}^{(q)},
\end{aligned}$$

and

$$\begin{aligned}
&\begin{bmatrix} A_{11p}^{(q)} & A_{21p}^{(q)} & A_{31p}^{(q)} & A_{41p}^{(q)} \\ A_{12p}^{(q)} & A_{22p}^{(q)} & A_{32p}^{(q)} & A_{42p}^{(q)} \\ A_{13p}^{(q)} & A_{23p}^{(q)} & A_{33p}^{(q)} & A_{43p}^{(q)} \\ A_{14p}^{(q)} & A_{24p}^{(q)} & A_{34p}^{(q)} & A_{44p}^{(q)} \end{bmatrix} = \left[D_p^{(q)} \right]^{-1} \\
\left[D_p^{(q)} \right] &= \begin{bmatrix} -\omega \xi_{m12}^{(q,p)} & i\omega \xi_{m1}^{(q,p)} & -\omega \mu_{12}^{(q,p)} & i\omega \mu_1^{(q,p)} \\ -i\omega \xi_{m1}^{(q,p)} & \omega \xi_{m12}^{(q,p)} & -i\omega \mu_1^{(q,p)} & -\omega \mu_{12}^{(q,p)} \\ \omega \varepsilon_{12}^{(q,p)} & -i\omega \varepsilon_1^{(q,p)} & \omega \xi_{e12}^{(q,p)} & -i\omega \xi_{e1}^{(q,p)} \\ i\omega \varepsilon_1^{(q,p)} & \omega \varepsilon_{12}^{(q,p)} & i\omega \xi_{e1}^{(q,p)} & \omega \xi_{e12}^{(q,p)} \end{bmatrix}. \quad (\text{A1})
\end{aligned}$$

APPENDIX 2.

To transform the scattered fields of g th cylinder ($g = 1, \dots, N$; $g \neq q$) with respect to $O_M^{(g)} \left(\rho_M^{(g)}, \varphi_M^{(g)}, z_M^{(g)} \right)$ to the q th coordinates $O_M^{(q)} \left(\rho_M^{(q)}, \varphi_M^{(q)}, z_M^{(q)} \right)$, we must have

$$H_n^{(2)} \left(k \rho_M^{(g)} \right) e^{in\varphi_M^{(g)}} = \sum_{m=-\infty}^{+\infty} H_{n-m}^{(2)} \left(k D_{qg} \right) J_m \left(k \rho_M^{(q)} \right) e^{i \left[m \varphi_M^{(q)} - (m-n) \varphi_{qg}' \right]}, \quad (\text{A2a})$$

and

$$D_{qg}^2 = \rho_q'^2 + \rho_g'^2 - 2\rho_q'\rho_g'\cos(\varphi_q' - \varphi_g'), \quad (\text{A2b})$$

$$\varphi_{qg} = \begin{cases} \cos^{-1}\left(\frac{\rho_q'\cos\varphi_q' - \rho_g'\cos\varphi_g'}{D_{qg}}\right), & \rho_q'\sin\varphi_q' \geq \rho_g'\sin\varphi_g', \\ -\cos^{-1}\left(\frac{\rho_q'\cos\varphi_q' - \rho_g'\cos\varphi_g'}{D_{qg}}\right), & \rho_q'\sin\varphi_q' < \rho_g'\sin\varphi_g'. \end{cases} \quad (\text{A2c})$$

APPENDIX 3.

Eq. (8)–(12) can be written as

$$\left[X_{11}^{(q)}\right]_{L \times L} \left[D_1^{(q)}\right]_{L \times 1} = \left[X_{12}^{(q)}\right]_{L \times L} \left[D_2^{(q)}\right]_{L \times 1}, \quad (\text{A3a})$$

$$\left[X_{22}^{(q)}\right]_{L \times L} \left[D_2^{(q)}\right]_{L \times 1} = \left[X_{23}^{(q)}\right]_{L \times L} \left[D_3^{(q)}\right]_{L \times 1}, \quad (\text{A3b})$$

$$\left[X_{pp}^{(q)}\right]_{L \times L} \left[D_p^{(q)}\right]_{L \times 1} = \left[X_{p(p+1)}^{(q)}\right]_{L \times L} \left[D_{p+1}^{(q)}\right]_{L \times 1}, \quad (\text{A3c})$$

$$\left[X_{(M-1)(M-1)}^{(q)}\right]_{L \times L} \left[D_{M-1}^{(q)}\right]_{L \times 1} = \left[X_{(M-1)M}^{(q)}\right]_{L \times L} \left[D_M^{(q)}\right]_{L \times 1}. \quad (\text{A3d})$$

Combining (A3a) with (A3b)–(A3d), we have

$$\left[D_M^{(q)}\right]_{L \times 1} = \left[X^{(q)}\right]_{L \times L}^{-1} \left[X_{11}^{(q)}\right]_{L \times L} \left[D_1^{(q)}\right]_{L \times 1}, \quad (\text{A4a})$$

where

$$\begin{aligned} \left[X^{(q)}\right]_{L \times L} &= \left[X_{12}^{(q)}\right] \left[X_{22}^{(q)}\right]^{-1} \cdots \left[X_{(p-1)p}^{(q)}\right] \left[X_{pp}^{(q)}\right]^{-1} \\ &\quad \cdots \left[X_{(M-1) \times (M-1)}^{(q)}\right]^{-1} \left[X_{(M-1)M}^{(q)}\right]. \end{aligned} \quad (\text{A4b})$$

ACKNOWLEDGMENT

This work has been supported by a research project RP3981676 from the National University of Singapore.

REFERENCES

1. Parriker, R. P., A. A. Kishk, and A. Z. Elsherbeni, "Scattering from an impedance cylinder embedded in a non concentric dielectric cylinder," *IEE Proc.-Microw. Antennas and Propagat.*, Vol. 138, No. 2, 169–175, 1991.
2. Kishk, A. A., R. P. Parriker, and A. Z. Elsherbeni, "Electromagnetic scattering from an eccentric multilayered circular cylinder," *IEEE Trans. Antennas and Propagat.*, Vol. 40, No. 3, 295–302, 1992.
3. Roumeliotis, J. A., and N. B. Kakogiannos, "Scattering from an infinite cylinder of small radius embedded into a dielectric one," *IEEE Trans. Microwave Theory and Tech.*, Vol. 42, No. 3, 463–469, 1994.
4. Stratigaki, L. G., M. P. Loamnidou, and D. P. Chrissoulidis, "Scattering from a dielectric cylinder with multiple eccentric cylindrical dielectric inclusions," *IEE Proc.-Microw. Antennas and Propagat.*, Vol. 143, No. 6, 505–511, 1996.
5. Tanyer, S. G., and R. G. Olsen, "High-frequency scattering by a conducting circular cylinder coated with a lossy dielectric of nonuniform thickness," *IEEE Trans. Antennas and Propagat.*, Vol. 45, No. 4, 689–697, 1997.
6. Bever, J. S., and J. P. Allebach, "Multiple scattering by a planar array of parallel dielectric cylinders," *Applied Optics*, Vol. 31, No. 18, 3524–3531, 1992.
7. Elsherbeni, A. Z., M. Hamid, and G. Tiau, "Iterative scattering of a Gaussian beam by an array of circular conducting and dielectric cylinders," *J. Electromagn. Waves and Appl.*, Vol. 7, 1323–1342, 1993.
8. Ohki, M., K. Shimizu, H. Sakurai, and S. Kozaki, "New expression for beam wave scattering in the case of various type of arbitrary scattering," *Int. J. Electron.*, Vol. 82, No. 4, 403–413, 1997.
9. Tsalamengas, J. L., "Interaction of electromagnetic waves with general bianisotropic slabs," *IEEE Trans. Microwave Theory and Tech.*, Vol. 40, No. 10, 1870–1878, 1992.
10. Olyslager, F., "Time-harmonic two- and three-dimensional Green's dyadics for general uniaxial bianisotropic media," *IEEE Trans. Antennas and Propagat.*, Vol. 43, No. 4, 430–434, 1995.
11. Olyslager, F., and B. Jakoby, "Time-harmonic two- and three-dimensional Green dyadics for a special class of gyrotropic bianisotropic media," *IEE Proc.-Microw. Antennas and Propagat.*, Vol. 143, No. 5, 413–416, 1996.

12. Lakhtakia, A., and W. S. Weiglhofer, "Further results on light propagation in helicoidal bianisotropic mediums: oblique propagation," *Proc. R. Soc. Lond. A*, 453, 93–105, 1997.
13. Yang, H.-Y., "A spectral recursive transmission method for electromagnetic waves in generalized anisotropic layered media," *IEEE Trans. Antennas and Propagat.*, Vol. 45, No. 3, 520–526, 1997.
14. Yang, H.-Y., and P. L. E. Uslenghi, "Theory of certain bianisotropic waveguide," *Radio Science*, Vol. 28, 919–927, 1993.
15. Xu, Y.-S., and R. G. Bosisio, "An efficient method for study of general bianisotropic waveguides," *IEEE Trans. Microwave Theory and Tech.*, Vol. 43, No. 4, 873–879, 1995.
16. Valor, L., and J. Zapata, "An efficient finite element formulation to analyze waveguides with lossy inhomogeneous bi-anisotropic materials," *IEEE Trans. Microwave Theory and Tech.*, Vol. 44, No. 2, 291–296, 1996.
17. Jakoby, B., and D. D. Zutter, "Analysis of guided waves in inhomogeneous bianisotropic cylindrical waveguides," *IEEE Trans. Microwave Theory and Tech.*, Vol. 44, No. 2, 297–310, 1996.
18. Graglia, R. D., M. S. Sarto, and P. L. E. Uslenghi, "TE and TM modes in cylindrical metallic structures filled with bianisotropic materials," *IEEE Trans. Microwave Theory and Tech.*, Vol. 44, No. 8, 1470–1477, 1996.
19. Olyslager, F., "Properties of and generalized full-wave transmission line models for hybrid (bi)(an)isotropic waveguides," *IEEE Trans. Microwave Theory and Tech.*, Vol. 44, No. 11, 2064–2309, 1996.
20. Uslenghi, P. L. E., "TE-TM decoupling for guided propagation in bianisotropic media," *IEEE Trans. Antennas and Propagat.*, Vol. 45, No. 2, 284–286, 1997.
21. Hanson, G. W., "A numerical formulation of dyadic Green's functions for planar bianisotropic media with application to printed transmission lines," *IEEE Trans. Microwave Theory and Tech.*, Vol. 44, No. 1, 144–151, 1996.
22. Olyslager, F., E. Laermans, and D. D. Zutter, "Rigorous quasi-TEM analysis of multiconductor transmission lines in bi-isotropic media-Part I: theoretical analysis for general inhomogeneous media and generalization to bianisotropic media," *IEEE Trans. Microwave Theory and Tech.*, Vol. 43, No. 7, 1409–1415, 1995.
23. Olyslager, F., E. Laermans, and D. D. Zutter, "Rigorous quasi-TEM analysis of multiconductor transmission lines in bi-isotropic media-Part II: numerical solution for layered media," *IEEE Trans. Microwave Theory and Tech.*, Vol. 43, No. 7, 1416–1423,

- 1995.
24. Whites, K. W., and C. Y. Chung, "Composite uniaxial bianisotropic chiral materials characterization: comparison of predicted and measured scattering," *J. Electromagn. Waves and Appl.*, Vol. 11, 377–387, 1997.
 25. Kluskens, M. S. and E. H. Newman, "Scattering from a chiral cylinder of arbitrary cross section," *IEEE Trans. Antennas and Propagat.*, Vol. 38, No. 9, 1448–1455, 1990.
 26. Kluskens, M. S., and E. H. Newman, "Scattering by a multilayer chiral cylinder," *IEEE Trans. Antennas and Propagat.*, Vol. 39, 91–96, 1991.
 27. Graglia, R. D., and P. L. E. Uslenghi, "Electromagnetic oblique scattering by a cylinder coated with chiral layers and anisotropic jump-immittance sheets," *J. Electromagn. Waves and Appl.*, Vol. 6, No. S/6, 695–720, 1992.
 28. Shen, Z.-X., "Electromagnetic scattering by an impedance cylinder coated eccentrically with a chiroplasma," *IEE Proc.-Microw. Antennas and Propag.*, Vol. 141, No. 4, 279–284, 1994.
 29. Majeed, A., Al-Kanhal, and E. Arvas, "Electromagnetic scattering from a chiral cylinder of arbitrary cross section," *IEEE Trans. Antennas and Propagat.*, Vol. 44, No. 7, 1996.
 30. Chen, Z.-N., and W. Hong, "Electromagnetic scattering from a chiral cylinder-general case," *IEEE Trans. Antennas and Propagat.*, Vol. 44, No. 7, 912–917, 1996.
 31. Jakoby, B., "Scattering of obliquely incident waves by an impedance cylinder with inhomogeneous bianisotropic coating," *IEEE Trans. Antennas and Propagat.*, Vol. 45, No. 4, 648–655, 1997.
 32. Konistis, K., and J. L. Tsalamengas, "Plane wave scattering by an array of bianisotropic cylinders enclosed by another one in an unbounded bianisotropic space: oblique incidence," *J. Electromagn. Waves and Appl.*, Vol. 11, 1073–1090, 1997.
 33. Yin, W. Y., "The features of Mueller scattering matrix for two penetrable composite Faraday chiral cylinder," *J. Electromagn. Waves and Appl.*, Vol. 10, 1199–1216, 1996.
 34. Yin, W. Y., H. L. Zhao, and W. Wan, "Parametric study on the scattering characteristics of two impedance cylinders eccentrically coated with Faraday chiral materials," *J. Electromagn. Waves and Appl.*, Vol. 10, 1467–1484, 1996.
 35. Yin, W. Y., "Scattering by a linear array of uniaxial bianisotropic chiral cylinders," *Micro. and Opt. Tech., Lett.*, Vol. 12, No. 5, 287–295, 1996.

36. Dmitriev, V. A., "Constitutive tensors and general properties of complex and bianisotropic media described by continuous groups of symmetry," *Electr. Lett.*, Vol. 34, No. 6, 532–534, 1998.
37. Dmitriev, V. A., "Group theoretical approach to determine structure of complex and composite media constitutive tensors," *Electr. Lett.*, Vol. 34, No. 8, 743–745, 1998.
38. Dmitriev, V. A., "Symmetry description of continuous homogeneous isotropic media under external perturbation," *Electr. Lett.*, Vol. 34, No. 8, 745–747, 1998.
39. Weiglhofer, W. S., and A. Lakhtakia, "The correct constitutive relations of chiroplasmas and chiroferrites," *Micro. Opt. Tech. Lett.*, Vol. 17, No. 6, 405–408, 1998.
40. Weiglhofer, W. S., "Scalar Green functions and superpotentials of a faraday chiral medium," *Inter. J. Electron. Commun. (AEÜ)*, Vol. 52, No. 2, 109–112, 1998.
41. Sahin, A., and E. L. Miller, "Recursive T-matrix methods for scattering from multiple dielectric and metallic objects," *IEEE Trans. Antennas and Propagat.*, Vol. 46, No. 5, 672–678, 1998.
42. Elsherbeni, A. Z., and A. A. Kishk, "Modeling of cylindrical objects by circular dielectric and conducting cylinders," *IEEE Trans. Antennas and Propagat.*, Vol. 40, No. 1, 96–99, 1992.